February 2006

Pope, D.N. and Gogos G. "A New Multicomponent Diffusion Formulation for the Finite-Volume Method: Application to Convective Droplet Combustion," Numerical Heat Transfer, Part B Fundamentals, Part B, 48, 3:213-234, (2005)

Numerical Heat Transfer, Part B, 48: 213–233, 2005

ISSN: 1040-7790 print/1521-0626 online
DOI: 10.1080/10407790590959807

Taylor & Francis
Taylor & Francis Group

A NEW MULTICOMPONENT DIFFUSION FORMULATION FOR THE FINITE-VOLUME METHOD: APPLICATION TO CONVECTIVE DROPLET COMBUSTION

Daniel N. Pope and George Gogos
Department of Mechanical Engineering, University of Nebraska–Lincoln, Lincoln, Nebraska, USA

A new multicomponent formulation, appropriate for use with the finite-volume method, has been developed to describe mass diffusion velocities accurately. The new formulation is applied in a quasi-steady numerical model for* n*-heptane fuel droplet combustion in a forced-convection environment. Results obtained using the complete formulation are compared to the results obtained under various assumptions. Using a single binary diffusion coefficient produces results for extinction velocity, maximum temperature, flame dimensions, evaporation constant, and drag coefficient that are significantly different from the results obtained using the complete formulation. Neglecting thermal diffusion (Soret effect) causes only minor changes (less than 2%).

1. INTRODUCTION

The numerical simulation of a multicomponent reacting flow requires the solution of the equations of mass, momentum, species, and energy conservation [1]. One of the most important methods used over the past few decades to solve the governing equations is the finite-volume method. In this method, all of the governing equations must be cast into a specific form; the diffusion term in each governing equation must be expressed as a gradient of the dependent variable for the equation [2]. All of the governing equations, with the exception of the species conservation equation, can be easily manipulated into the appropriate form. The diffusion term in the species conservation equation is based on the solution for the diffusion velocity. A general expression for the diffusion velocity includes the effects of the gradients in temperature (Soret effect), pressure, and species concentration, as well as the effect of the nonuniformity in the body forces [1]. The effect of pressure gradients on the diffusion velocity is usually negligible unless the flow Mach number

Received 9 June 2004; accepted 3 February 2005.
This research was partially funded by NASA EPSCoR under Grant NCC5-401 and ARO EPSCoR under Grant DAAD19-99-1-0116. Computational resources were provided by the Thermal/Fluids Computational Facility at the University of Nebraska–Lincoln.
The present address of Daniel N. Pope is University of Minnesota Duluth, Department of Mechanical and Industrial Engineering, 105 VKH, 1305 Ordean Court, Duluth, MN 55812-3042, USA.
Address correspondence to George Gogos, University of Nebraska–Lincoln, Department of Mechanical Engineering, N104 Walter Scott Engineering Center, Lincoln, NE 68588-0656, USA. E-mail: ggogos@unl.edu

NOMENCLATURE

a	fuel concentration exponent in reaction rate equation
A	preexponential factor
b	oxygen concentration exponent in reaction rate equation
c_p	specific heat capacity at constant pressure
C_D	drag coefficient
d	droplet diameter
D_{ij}	binary diffusion coefficient for the i–j pair
D_{im}	effective diffusion coefficient for the ith species
$D_{T,i}$	thermal diffusion coefficient for the ith species
E_a	activation energy
g	gravitational acceleration
h	specific enthalpy
K	evaporation constant
k	thermal conductivity or Boltzmann's constant
k_T	thermal diffusion ratio
L	latent heat of vaporization
$\dot{m}''_\theta$	local mass flux at droplet surface
N	total number of chemical species
p	pressure
r	radial position
R	droplet radius
Re_∞	Reynolds number
R_f	ideal gas constant for fuel
R_u	universal gas constant
T	temperature
T_c	critical temperature
U_∞	free-stream velocity
V_c	critical volume
$\vec{V}_i$	diffusion velocity of the ith species
$\vec{V}_i$	component of $\vec{V}_i$ caused by concentration gradient
$\vec{\mathbf{V}}_i^0$	zeroth order approximation of $\vec{\mathbf{V}}_i$
$\vec{v}$	velocity vector
v_r	velocity component in radial direction
v_θ	velocity component in polar direction
$\bar{W}$	average molecular weight
W_i	molecular weight of ith species
$\vec{\mathbf{W}}_i$	component of $\vec{V}_i$ caused by temperature gradient
X_i	mole fraction of ith species
Y_i	mass fraction of ith species
$\delta\vec{\mathbf{V}}_i$	correction velocity for $\vec{\mathbf{V}}_i$
ϵ	characteristic energy parameter
θ	polar position
μ	dynamic viscosity
ν	kinematic viscosity
ν''_i, ν'_i	stoichiometric coefficient of the ith product and reactant, respectively
ρ	density
σ	collision diameter
ω_i	rate of mass production of the ith species per unit volume.
Ω	collision integral

Subscripts

e	at extinction
f	fuel or flame
g	gas phase
i	ith species
l	liquid phase
o	oxygen (O_2)
ref	reference state
s	droplet surface
sat	saturated liquid/vapor
∞	free-stream or outer computational boundary

Superscripts

*	dimensionless variable

is high, and in most applications, the only body force is gravity (uniform). The resulting equation for the diffusion velocity contains the species concentration and temperature gradients. The finite-volume form of the species conservation equation requires an expression for the diffusion velocity in terms of the gradient of the species mass fraction. Thus, a direct solution for the diffusion velocity would be inappropriate.

The assumption of negligible thermal diffusion (Soret effect) coupled with Fick's law for diffusion has been employed in the past to manipulate the diffusion velocity into a form appropriate for use with the finite-volume method. In addition, the diffusion coefficient used in Fick's law has ranged from a single binary diffusion coefficient for all species (e.g., Huang and Chen [3]) to various forms of an

"effective" diffusion coefficient for a given species into the mixture of all other species (e.g., Takeda and Hishida [4]). The authors are unaware of the incorporation of a rigorous formulation for the diffusion velocity in finite-volume numerical simulations available in the literature.

This article presents a new multicomponent formulation that is appropriate for use with the finite-volume method. The governing equations for the diffusion velocity are derived and incorporated in a quasi-steady numerical model for *n*-heptane droplet combustion in a forced-convection environment. The model has been extensively validated via comparison to both experimental and theoretical results available in the literature. Numerical results obtained using the complete formulation are compared to the results obtained while assuming (1) thermal diffusion is negligible and (2) thermal diffusion is negligible and all binary diffusion coefficients are the same. The effect these assumptions have on the extinction velocity and on the results at a fixed Reynolds number ($\mathrm{Re}_\infty = 10$) is investigated for a 1.3-mm-diameter droplet in a low-(300 K) and a high-(1,200 K) temperature environment at atmospheric pressure.

2. DIFFUSION VELOCITY TREATMENT

The "standard form" for the governing equations in the finite-volume method [2] can be written as

$$\frac{\partial}{\partial t}(\rho\Phi) + \nabla \cdot (\rho\vec{v}_c\Phi) = \nabla \cdot (\Gamma\nabla\Phi) + S \tag{1}$$

where t is time, ρ is the density, Φ is the dependent variable, $\vec{v}_c$ is the convection velocity, Γ is the diffusion coefficient, and S is the source term. The governing equations for a multicomponent reacting flow given by Williams [1] can be easily placed in the required form with the exception of the conservation of species equation. The species conservation equation, in terms of the mass fraction of the ith species (Y_i), is

$$\frac{\partial}{\partial t}(\rho Y_i) + \nabla \cdot (\rho\vec{v}Y_i) = \omega_i - \nabla \cdot (\rho Y_i\vec{V}_i) \tag{2}$$

where $\vec{v}$ is the mass-average velocity, ω_i is the rate of mass production of the ith species per unit volume, and $\vec{V}_i$ is the diffusion velocity of the ith species.

In order to place Eq. (2) in the same form as Eq. (1), $\vec{V}_i$ must be described in terms of the gradient of Y_i. Adopting the standard assumptions of (1) no variation in the body force per unit mass (e.g., the only body force is gravity) and (2) mass diffusion due to a pressure gradient is negligible, the governing equation for the diffusion velocity in a mixture of N gases is given by Williams [1] as

$$\nabla X_i = \sum_{j=1}^{N}\left(\frac{X_iX_j}{\mathrm{D}_{ij}}\right)(\vec{V}_j - \vec{V}_i) + \sum_{j=1}^{N}\left[\left(\frac{X_iX_j}{\rho\mathrm{D}_{ij}}\right)\left(\frac{D_{T,j}}{Y_j} - \frac{D_{T,i}}{Y_i}\right)\right]\left(\frac{\nabla T}{T}\right) \tag{3}$$

where T is the temperature, X_i and $D_{T,i}$ are the mole fraction and thermal diffusion coefficient of the ith species, respectively, and D_{ij} is the binary diffusion coefficient

for the i–j species pair. The above equation states that mass diffusion consists of two components: "ordinary" diffusion, which is mass diffusion due to concentration gradients; and "thermal" diffusion (also known as the Soret effect), which is mass diffusion caused by temperature gradients. The N diffusion velocities in Eq. (3) are subject to the constraint

$$\sum_{i=1}^{N} Y_i \vec{V}_i = 0 \tag{4}$$

and the thermal diffusion coefficient has the following property [5]:

$$\sum_{i=1}^{N} D_{T,i} = 0 \tag{5}$$

The total diffusion velocity of the ith species can be written as

$$\vec{V}_i = \vec{\mathbf{V}}_i + \vec{\mathbf{W}}_i \tag{6}$$

where $\vec{\mathbf{V}}_i$ is the component due to "ordinary" diffusion and $\vec{\mathbf{W}}_i$ is the component due to "thermal" diffusion. The thermal diffusion velocity can be determined by inspection from Eqs. (3) and (6):

$$\vec{\mathbf{W}}_i = -\frac{D_{T,i}}{\rho Y_i} \frac{\nabla T}{T} \tag{7}$$

The use of Eqs. (5)–(7) in Eqs. (3) and (4) leads to the following expression for the "ordinary" diffusion velocities:

$$\nabla X_i = \sum_{j=1}^{N} \left(\frac{X_i X_j}{\mathrm{D}_{ij}} \right) (\vec{\mathbf{V}}_j - \vec{\mathbf{V}}_i) \tag{8}$$

which are subject to the constraint

$$\sum_{i=1}^{N} Y_i \vec{\mathbf{V}}_i = 0 \tag{9}$$

Equation (8) is often referred to as the Stefan-Maxwell equation [1, 6] and it, along with the constraint Eq. (9), will be used as a starting point for the discussion that follows.

Using a procedure that is similar to that used by Oran and Boris [7, 8], the "ordinary" diffusion velocity is divided into a zeroth-order approximation ($\vec{\mathbf{V}}_i^0$) and a correction velocity ($\delta\vec{\mathbf{V}}_i$):

$$\vec{\mathbf{V}}_i = \vec{\mathbf{V}}_i^0 + \delta\vec{\mathbf{V}}_i \tag{10}$$

The zeroth-order approximation to the "ordinary" diffusion velocity corresponds to the diffusion of species i into the mixture of all other species and is given by

$$\vec{\mathbf{V}}_i^0 = -\frac{D_{im}}{Y_i}\nabla Y_i \tag{11}$$

where

$$D_{im} = \frac{1 - X_i}{\sum_{j\neq i}(X_j/\mathrm{D}_{ij})} \tag{12}$$

is the effective diffusion coefficient for the ith species into the mixture of all other species (see, e.g., [5] and Method V in [9]). Using the identities $\sum Y_i = 1$ and $X_i = (Y_i/W_i)/\sum(Y_j/W_j)$ (where W_i is the molecular weight of the ith species) in the above equations and rearranging gives an expression for the correction velocities

$$\delta\vec{\mathbf{V}}_i \sum_{j\neq i}\frac{Y_j}{W_j\mathrm{D}_{ij}} - \sum_{j\neq i}\frac{Y_j}{W_j\mathrm{D}_{ij}}\delta\vec{\mathbf{V}}_j = \sum_{j\neq i}\frac{1}{W_j}\left(1 - \frac{D_{jm}}{\mathrm{D}_{ij}}\right)\nabla Y_j \tag{13}$$

which are subject to the constraint

$$\sum_{i=1}^{N} Y_i\delta\vec{\mathbf{V}}_i = \sum_{i=1}^{N} D_{im}\nabla Y_i \tag{14}$$

The N Eq. (13) are not linearly independent and therefore Eq. (14) must replace one of the equations in the solution. Adopting an iterative solution technique, as is customarily employed in the finite-volume method, introduces the requirement of a diagonally dominant coefficient matrix to guarantee solution convergence. Equation (13) is already in diagonally dominant form. Equation (14) is only diagonally dominant when the equation is applied to the ith species in a binary system with $Y_i \geq 0.5$. Using the identity $\sum Y_i = 1$, Eq. (14) may be written as

$$\delta\vec{\mathbf{V}}_i + \sum_{j\neq i} Y_j\delta\vec{\mathbf{V}}_j = \sum_{j=1}^{N} D_{jm}\nabla Y_j + \delta\vec{\mathbf{V}}_i^p(1 - Y_i) \tag{15}$$

where the superscript p indicates the value from the previous iteration. By analogy to the binary case, Eq. (15) should be employed for the species with the maximum Y_i. It can be shown that the simultaneous solution of Eqs. (13) and (15) results in $\delta\vec{\mathbf{V}}_i = 0$; $i = 1, \ldots, N$ for both a binary system ($N = 2$) and a system with $N > 2$ when all binary diffusion coefficients are equal ($\mathrm{D}_{ij} = \mathrm{D}$).

Application of the above formulation to the conservation of species Eq. (2) results in the following equation:

$$\frac{\partial}{\partial t}(\rho Y_i) + \nabla\cdot[\rho(\vec{v} + \delta\vec{\mathbf{V}}_i + \vec{\mathbf{W}}_i)Y_i] = \nabla\cdot(\rho D_{im}\nabla Y_i) + \omega_i \tag{16}$$

which is appropriate for use with the finite-volume method. Because the present formulation exactly satisfies the constraint Eq. (4), the summation of the species conservation equations is identically equal to the continuity equation, and the divergence-free constraint is satisfied. Equation (16) indicates that each species has an effective convection velocity of $\vec{v} + \delta\vec{V}_i + \vec{W}_i$. It is appropriate to use this effective convection velocity when discretizing the species conservation equations using the upwind scheme or other related schemes. Mathematically, the new velocities ($\delta\vec{V}_i$ and $\vec{W}_i$) behave in the same manner as the mass-average velocity. Physically, the temperature gradient and the difference in ordinary diffusion velocities between adjacent grid points will cause a "shift" in the gradient of the species mass fraction.

3. THEORETICAL MODEL

A previously developed model for quasi-steady droplet combustion, which utilized a single binary diffusion coefficient [10], has been modified to include the current multicomponent formulation and the effect of gravity. The model simulates the evaporation/combustion of a liquid fuel droplet of radius R in a convective, low-pressure environment of infinite expanse (Figure 1). The free-stream pressure (p_∞), temperature (T_∞), and velocity (U_∞) are constant. The model assumes a quasi-steady gas phase [11] with variable properties. Interaction between the gas and liquid at the interface causes circulation within the droplet and evaporation from the droplet surface. The liquid-phase quasi-steady equations with constant properties are incorporated to account for internal circulation and tangential velocities at the droplet surface. Other assumptions used to make the problem more tractable include: (1) the flow is axisymmetric and laminar; (2) the droplet maintains a spherical shape; (3) thermal radiation is negligible; (4) the Dufour effect and mass diffusion due to a pressure gradient, which are second-order effects, are negligible; (5) viscous dissipation and pressure work are negligible; (6) gas-phase transport and thermodynamic properties are a function of temperature and composition only; (7) the fuel droplet consists of a single component with negligible solubility of gas-phase species into the liquid phase; and (8) heat transfer to the droplet interior is negligible. The gas phase consists of several different chemical species, the number and type of which are

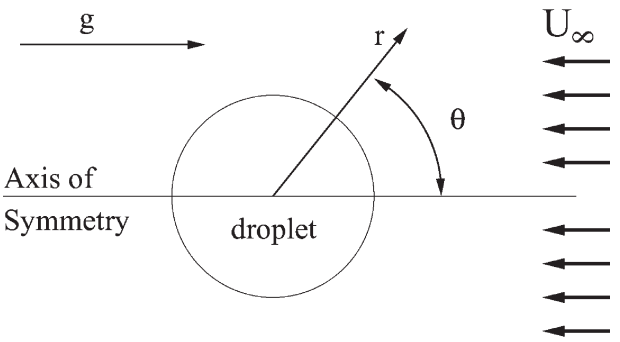

Figure 1. Problem schematic (buoyancy-induced flow aiding forced convection).

defined by the chosen fuel, the composition of the ambient gases, and the chemical kinetics model that is employed.

The governing equations for the gas and liquid phases based on the above assumptions are shown below in vector form.

3.1. Gas Phase

Continuity:

$$\nabla \cdot (\rho \vec{v}) = 0 \tag{17}$$

Conservation of species:

$$\nabla \cdot [\rho(\vec{v} + \delta \vec{\mathbf{V}}_i + \vec{\mathbf{W}}_i) Y_i] = \nabla \cdot (\rho D_{im} \nabla Y_i) + \omega_i \tag{18}$$

Momentum conservation:

$$\rho \vec{v} \cdot \nabla \vec{v} = -\nabla p - \nabla \left[\frac{2}{3} \mu (\nabla \cdot \vec{v}) \right] + \nabla \cdot \left\{ \mu \left[(\nabla \vec{v}) + (\nabla \vec{v})^T \right] \right\} + \rho \vec{g} \tag{19}$$

Energy conservation:

$$\nabla \cdot (\rho \vec{v} T) = \nabla \cdot \left(\frac{k}{c_p} \nabla T \right) + \frac{k}{{c_p}^2} \nabla T \cdot \nabla c_p - \frac{1}{c_p} \sum_{i=1}^{N} \rho Y_i \vec{V}_i \cdot \nabla h_i - \frac{1}{c_p} \sum_{i=1}^{N} \omega_i h_i \tag{20}$$

3.2. Liquid Phase

Continuity:

$$\nabla \cdot \vec{v} = 0 \tag{21}$$

Momentum conservation:

$$\rho \vec{v} \cdot \nabla \vec{v} = -\nabla p + \mu \nabla^2 \vec{v} + \rho \vec{g} \tag{22}$$

3.3. Interface Conditions

The gas-phase and liquid-phase governing equations are coupled at the interface by the following equations, which are shown in spherical coordinates.
Continuity of tangential velocities:

$$v_{\theta,g,s} = v_{\theta,l,s} \tag{23}$$

Continuity of shear stress:

$$\mu_{g,s} \left(\frac{\partial v_{\theta,g}}{\partial r} - \frac{v_{\theta,g}}{r} + \frac{1}{r} \frac{\partial v_{r,g}}{\partial \theta} \right)_s = \mu_{l,s} \left(\frac{\partial v_{\theta,l}}{\partial r} - \frac{v_{\theta,l}}{r} + \frac{1}{r} \frac{\partial v_{r,l}}{\partial \theta} \right)_s \tag{24}$$

Conservation of species:

$$\text{Fuel: } \dot{m}''_\theta = \dot{m}''_\theta Y_{f,s} + \rho_{g,s} Y_{f,s} V_{r,f,s} \tag{25}$$

$$\text{Nonfuel: } 0 = \dot{m}''_\theta Y_{i,s} + \rho_{g,s} Y_{i,s} V_{r,i,s} \tag{26}$$

Conservation of energy:

$$\dot{m}''_\theta L = k_{g,s} \left.\frac{\partial T_g}{\partial r}\right|_s \tag{27}$$

Conservation of mass:

$$\dot{m}''_\theta = \rho_{g,s} v_{r,g,s} = \rho_{l,s} v_{r,l,s} \tag{28}$$

Phase equilibrium is assumed at the droplet surface. The Clausius-Clapeyron equation is employed to relate the gas-phase surface temperature ($T_{g,s}$) to the partial pressure of the fuel in the gas phase ($p_{g,f,s}$).

$$\ln\left[\frac{p_{g,f,s}}{p_{\text{ref,sat}}}\right] = \frac{L}{R_f}\left[\frac{1}{T_{\text{ref,sat}}} - \frac{1}{T_{g,s}}\right] \tag{29}$$

3.4. Boundary Conditions

The boundary conditions in terms of spherical coordinates are listed below.

Inflow: $r = r_\infty,\ 0 \le \theta \le \pi/2$

$$\begin{aligned} v_r &= -U_\infty \cos\theta \\ v_\theta &= U_\infty \sin\theta \\ T &= T_\infty \\ p &= p_\infty \\ Y_i &= Y_{i,\infty} \qquad i = 1, \ldots, N \end{aligned}$$

Outflow: $r = r_\infty,\ \pi/2 < \theta \le \pi$

$$\frac{\partial v_\theta}{\partial r} = \frac{\partial T}{\partial r} = \frac{\partial p}{\partial r} = \frac{\partial Y_i}{\partial r} = 0$$

v_r is extrapolated using the continuity equation

Axis of symmetry: $\theta = 0$ or π

$$\begin{aligned} v_\theta &= 0 \\ \frac{\partial v_r}{\partial \theta} &= \frac{\partial T}{\partial \theta} = \frac{\partial p}{\partial \theta} = \frac{\partial Y_i}{\partial \theta} = 0 \end{aligned}$$

3.5. Combustion Model

The fuel is *n*-heptane, which is oxidizing in dry air. A one-step overall reaction is utilized,

$$C_7H_{16} + 11(O_2 + 3.77N_2) \longrightarrow 7CO_2 + 8H_2O + 11(3.77N_2)$$

with the associated finite-rate chemical kinetics defined by

$$\omega_i = W_i(\nu_i'' - \nu_i')A\left(\frac{\rho Y_f}{W_f}\right)^a\left(\frac{\rho Y_o}{W_o}\right)^b \exp\left(\frac{-E_a}{R_u T}\right) \tag{30}$$

where ω_i is the rate of mass production of the ith species per unit volume, A is the preexponential factor, E_a is the activation energy, and a and b are the fuel and oxygen concentration exponents, respectively.

The values for the kinetics parameters (A, E_a, a, and b) for a one-step overall reaction are determined empirically. Seiser et al. [12] suggest the following values for *n*-heptane: $A = 7.07 \times 10^{11}\,(\text{kmol/m}^3)^{1-a-b}/\text{s}$, $E_a = 1.53 \times 10^5\,\text{kJ/kmol}$, $a = 1.0$, and $b = 1.0$. Seiser et al. measured strain rate at extinction as a function of oxygen concentration for nonpremixed flames stabilized in an oxidizer stream counterflowing over a liquid pool of *n*-heptane. The given kinetics parameters resulted in a match between their numerical predictions and experimental data. However, the experimental data were obtained under normal gravity and the numerical model neglected gravity. Like Seiser et al. [12], the current work assumes that the reaction is first-order with respect to fuel and oxygen ($a = b = 1$). Appropriate values for A and E_a were determined by matching normal-gravity experimental data available in the literature with normal-gravity numerical results (see Results section).

3.6. Properties

Variable properties in the gas phase were calculated using the ideal gas law and low-pressure correlations from Reid et al. [13]. Species viscosities and thermal conductivities were calculated using the method of Chung et al. [13, 14]. Mixture viscosity and thermal conductivity were obtained using the method of Wilke [13, 15]. The curvefits of McBride et al. [16] were used to calculate the species-specific heat capacities and enthalpies with the corresponding values for the mixture given by $c_p = \sum Y_i c_{p,i}$ and $h = \sum Y_i h_i$. The binary diffusion coefficients D_{ij} were evaluated using the first approximation from kinetic theory [13, 17] and the Lennard-Jones 12–6 potential.

Methods for calculating the thermal diffusion coefficient $D_{T,i}$ based on kinetic theory [17, 18] are computationally intensive. An approximation developed by Ramshaw [19] was used to calculated $D_{T,i}$ in the gas phase. For a mixture of ideal gases at a single temperature, the Ramshaw approximation can be written as

$$\frac{\bar{W}}{W_i \rho}\sum_{j\neq i}\frac{1}{W_j D_{ij}}(Y_j D_{T,i} - Y_i D_{T,j}) = \sum_{j\neq i}(\alpha_{ji} - \alpha_{ij}) \tag{31}$$

where

$$\alpha_{ij} = F_{ij}\left(W_j^2 \sum_{k=1}^{N} \frac{Y_k}{W_k} \sigma_{jk}^2 \sqrt{\frac{W_j + W_k}{W_j W_k}} \right)^{-1}$$

and

$$F_{ij} = \frac{1}{3} Y_i Y_j \sigma_{ij}^2 \sqrt{\frac{W_i + W_j}{W_i W_j}} \frac{W_i W_j}{(W_i + W_j)^2} \left(10\Omega_{i,j}^{(1,1)^*} - 12\Omega_{i,j}^{(1,2)^*} \right)$$

In the above equations, $\bar{W} = (\sum Y_i / W_i)^{-1}$ is the average molecular weight, $\sigma_{ij} = 0.5(\sigma_i + \sigma_j)$ is the collision diameter for the i–j pair in Å, $\Omega_{i,j}^{(1,1)^*}$ and $\Omega_{i,j}^{(1,2)^*}$ are collision integrals [20] evaluated at $T_{ij}^* = T(k/\epsilon_{ij})$, and the parameter (k/ϵ_{ij}) is given by

$$\frac{k}{\epsilon_{ij}} = \left(\sqrt{\frac{\epsilon_i}{k} \frac{\epsilon_j}{k}} \right)^{-1}$$

The collision diameter (σ_i) in Å and the parameter (ϵ_i/k) are estimated using [13]

$$\sigma_i = 0.809 V_{c,i}^{1/3} \text{ and } \frac{\epsilon_i}{k} = \frac{T_{c,i}}{1.2593}$$

where $V_{c,i}$ is the critical volume of the ith species in cm^3/mol and $T_{c,i}$ is the critical temperature of the ith species in K. The thermal diffusion coefficients are obtained via the simultaneous solution of $N - 1$ equations (31) subject to the constraint equation (5).

The approximation for $D_{T,i}$ used in the present work was tested to ensure that the thermal diffusion coefficients have the proper sign and magnitude. The calculated thermal diffusion ratio (k_T) for a binary sytem ($i = 1, 2$), which can be expressed as

$$k_T = \frac{\bar{W}^2}{\rho W_1 W_2} \frac{D_{T,1}}{\mathrm{D}_{12}}$$

was compared to results obtained using the first approximation from kinetic theory ($[k_T]_1$) given by Hirschfelder et al. [17]. All possible pairs of the five chemical species used in the combustion model were considered. For each species pair, Y_1 was varied from 0.1 to 0.9 in 0.1 increments and T was varied from 300 to 3,100 K in increments of 200 K. The ratio $k_T/[k_T]_1$ was within the range $0.4 \leq k_T/[k_T]_1 \leq 1.7$ for all of the cases.

The constant properties in the liquid phase were evaluated at the average surface temperature of the droplet. Values for the fuel density and viscosity were calculated using the correlations given by Haywood [21]. The latent heat of vaporization for the fuel was determined using the method of Pitzer et al. [13].

3.7. Supplemental Equations

The evaporation constant (K) and the drag coefficient (C_D) are presented in the Results section. The evaporation constant is given by

$$K = \frac{4R}{\rho_l} \int_0^{\pi} \dot{m}''_{\theta} \sin\theta \, d\theta$$

The drag coefficient and friction (F_F), pressure (F_P), and thrust (F_T) forces are evaluated as follows:

$$C_D = \frac{2(F_P + F_F + F_T)}{\rho_\infty U_\infty^2 \pi R^2}$$

$$F_F = 2\pi R^2 \int_0^{\pi} (\tau_{r\theta,g} \sin\theta - \tau_{rr,g} \cos\theta)_s \sin\theta \, d\theta$$

$$F_P = 2\pi R^2 \int_0^{\pi} p_{g,s} \cos\theta \, \sin\theta \, d\theta$$

$$F_T = 2\pi R^2 \int_0^{\pi} \dot{m}''_{\theta} (v_{r,g} \cos\theta - v_{\theta,g} \sin\theta)_s \sin\theta \, d\theta$$

where τ_{rr} and $\tau_{r\theta}$ are components of the shear stress tensor and the subscripts g and s denote evaluation in the gas phase and at the droplet surface, respectively.

4. NUMERICAL METHODS

The governing equations discussed in the previous section are discretized using the finite-volume [2] and SIMPLEC [22] methods. Convection/diffusion is modeled using the central difference with deferred correction method [21], with the "active" coefficients calculated using the power-law scheme [2]. A staggered grid is adopted to avoid zigzag pressure distributions. Relaxation is incorporated via an artificial time step that is embedded in the discretization equations. Hyperbolic tangent stretching functions [23] are used to concentrate grid points near the fore and aft lines of symmetry and at the droplet surface in both the gas phase and the liquid phase.

The discretization equations, with the exception of the diffusion velocity corrections, are solved using the alternating direction implicit (ADI) method with the tridiagonal matrix algorithm (TDMA) used on each line of the two alternating directions. A single global iteration consists of: (1) solution of the gas-phase discretization equations, (2) solution of the interface equations, (3) solution of the liquid-phase discretization equations, and (4) updating of the gas and liquid transport properties. The order of solution in the gas phase is (1) solve the momentum equations, (2) solve the pressure-correction equation, (3) correct the velocities and pressures, (4) solve for the diffusion velocity corrections, (5) solve the conservation of energy equation, (6) solve the first $N-1$ species conservation equations, and (7) solve for Y_N using $\sum Y_i = 1$. The solution procedure for the liquid phase is identical to steps (1)–(3)

for the gas phase. Global convergence is defined as follows; for $\Phi_{i,j} \geq \Phi^{\max} \times 10^{-3}$,

$$\left| \frac{\Phi_{i,j} - \Phi_{i,j}^{p}}{\Phi_{i,j}} \right| \leq 1.0 \times 10^{-4} \tag{32}$$

otherwise,

$$\left| \frac{\Phi_{i,j} - \Phi_{i,j}^{p}}{\Phi^{\max} \times 10^{-3}} \right| \leq 1.0 \times 10^{-4} \tag{33}$$

where Φ is $v_{r,g}$, $v_{\theta,g}$, T_g, $v_{r,l}$, or $v_{\theta,l}$, and $\Phi^{\max}$ is the maximum velocity or temperature in the given phase. Equation (33) is included to allow for convergence when velocities near zero exist in the computational domain.

The $N - 1$ equations (13) along with the constraint equation (15), which define the diffusion velocity corrections, are solved at each grid point using Gauss-Seidel iteration. Equation (15) is used for the correction velocity that corresponds to the species with the maximum Y_i.

Droplet ignition is accomplished numerically by assuming an initial condition of a chemically frozen environment with a high-temperature region surrounding the droplet. The velocities are initially set to zero in the computational domain. The fuel and oxygen mass fractions (Y_f and Y_o) are set as shown in Figure 2*a*, with nitrogen (N_2) making up the balance of the total mass ($Y_{N_2} = 1 - Y_o - Y_f$). The assumed initial temperature distribution is shown in Figure 2*b*. The values for r_1 and r_2 are adjustable program inputs which are varied until droplet ignition is achieved. When ignition occurs, results are independent of r_1 and r_2.

The extinction velocity ($U_{\infty,e}$) is determined by selecting an initial free-stream velocity that resulted in an envelope flame and then incrementing the free-stream velocity by 1 cm/s between successive quasi-steady solutions until a significant decrease in the evaporation constant is obtained. This particular definition of extinction is consistent with experimental observations of the change in mass burning rate at extinction [24, 25]. Physically, the extinction velocity corresponds to the maximum free-stream velocity that will support an envelope flame.

The computer code developed for this study was extensively tested prior to its use for combustion simulations. Problems of increasing complexity were employed in the testing procedure, which included the determination of minimum grid requirements. The details of the testing procedure and specific results are given in [10]. A brief summary of the testing procedure is provided below.

The gas-phase momentum, energy, and pressure-correction equations were tested via comparison of the program output to numerical and experimental results for constant-property flow over a sphere. The following data were used. (1) Drag coefficients for solid spheres at Reynolds numbers ($\mathrm{Re}_\infty = dU_\infty/\nu_\infty$) of 0.1, 1, 10, 100, and 300 were compared to numerical results in the literature [26–30] and to the correlations of Clift et al. [31]. (2) The dimensions of the attached vortex on the downstream side of the sphere were compared to the experimental results of Taneda [32] reported in [31]. (3) The angular location along the sphere surface at which the flow separates was compared to the correlation given by Clift et al. [31].

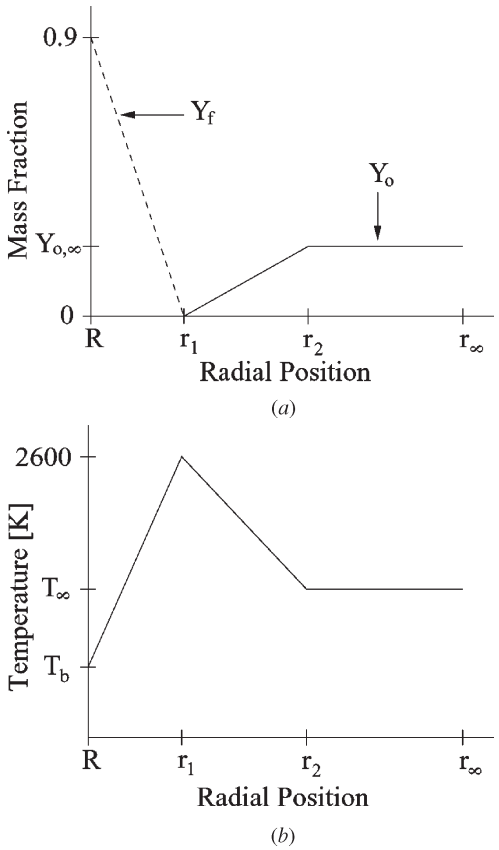

Figure 2. Initial conditions for fuel and oxygen mass fractions (*a*) and temperature distribution (*b*) as a function of radial position.

(4) Nusselt numbers for a Prandtl number of 0.672 and a dimensionless sphere temperature (T_s/T_∞) of 0.25 at Reynolds numbers of 0.1, 1, 10, and 50 were compared to the numerical results of Sayegh and Gauvin [29]. (5) Drag coefficients for blowing spheres at Reynolds numbers of 1 and 100 and blowing numbers ($\Lambda = v_{r,s}/U_\infty$) of 0.1 and 0.3 were compared to the numerical results of Cliffe and Lever [33].

The liquid-phase momentum and pressure-correction equations were tested by comparing results to the numerical predictions for isothermal flow past a water droplet of LeClair et al. [34]. Values for the location of the vortex in the liquid phase and the location and magnitude of the maximum velocity along the droplet surface were compared for Reynolds numbers of 30, 100, and 300.

The assembled code was also tested via comparison to the drag correlations of Chiang et al. [35] and Renksizbulut and Yuen [36], and to the Nusselt number correlations of Chiang et al. [35] and Renksizbulut and Yuen [37] for droplet evaporation. Combustion was disabled in the code to obtain the results for droplet

evaporation. Drag coefficients and Nusselt numbers for a 0.5-mm-diameter *n*-heptane droplet evaporating in air at temperatures of 800 and 1,200 K were compared to the correlations over a range of Reynolds numbers from 5 to 100.

The results from the current code were in excellent agreement with all of the test cases listed in the preceding paragraphs. There were some slight differences in the evaporation data, with the two correlations bracketing results for drag coefficient from the current code and the current code predicting slightly lower Nusselt numbers (a maximum of 10% at $\mathrm{Re}_\infty = 5$) than both correlations (see Pope [10] for details). These slight differences are probably due to the use of different property correlations.

Grid-generation parameters that can be adjusted within the model include the number of grid points in the polar direction (n_θ), the number of radial grid points in the gas phase and the liquid phase ($n_{r,g}$ and $n_{r,l}$), the dimensionless location of computational infinity ($r^*_\infty = r_\infty/R$), and the dimensionless grid spacing next to the droplet surface ($\Delta r^*_s = \Delta r_s/R$). These parameters were set to $n_\theta = 60$, $n_{r,g} = 250$, $n_{r,l} = 25$, $r^*_\infty = 50$, and $\Delta r^*_s = 0.02$ for the zero-gravity solutions given in the present work. The values for these parameters were tested to ensure the "grid independence" of the solutions.

5. RESULTS

The current work is concerned primarily with presenting the new multicomponent formulation for the finite-volume method. The interested reader is directed to articles by Pope and Gogos [38] and Pope et al. [39], which present extensive comparisons of numerical results with experimental data for droplet extinction (quasi-steady) and transient droplet combustion, respectively. Numerical results for quasi-steady droplet combustion and the effect of various "standard" assumptions on the results are discussed in the remainder of this section.

The experimental results of Gollahalli and Bruzstowski [40] and Goldsmith [41] for the extinction velocities of *n*-heptane droplets under normal gravity were used to determine appropriate values for A and E_a in the combustion model. In both sets of experiments, the buoyancy-induced flow aided the forced-convection flow (see Figure 1). Gollahalli and Brzustowski [40] used a porous sphere of diameter $d = 6$ mm to determine the extinction velocity as a function of ambient pressure. Their experiments utilized *n*-heptane as the fuel and "room"-temperature air as the oxidizer. They report an extinction velocity of approximately 0.5 m/s at a pressure of 1 atm. Goldsmith [41] utilized suspended fuel droplets with diameters between 1.5 and 1.8 mm in his experiments. He indicated that an envelope flame was not present at velocities above 0.345 m/s for a *n*-heptane droplet in air at "room" temperature and atmospheric pressure. Numerical simulations were conducted with $T_\infty = 300$ K, $p_\infty = 1$ atm, $g = 9.8\ \mathrm{m/s^2}$, and the buoyancy-induced flow aiding the forced convection. Use of the kinetics parameters $A = 3.35 \times 10^{11}\ \mathrm{m^3/kmol\,s}$, $E_a = 1.53 \times 10^5\ \mathrm{kJ/kmol}$, $a = 1.0$, and $b = 1.0$ in the numerical model resulted in predicted extinction velocities of 0.35 and 0.5 m/s for $d = 1.65$ and $d = 6$ mm, respectively. The above kinetics parameters were used to generate the remainder of the results given in the present work. A comparison of predicted extinction velocity with the experimental result of Okajima and Kumagai [42] is presented below.

For *n*-heptane and benzene droplets of approximately 1.3 mm in diameter, Okajima and Kumagai [42] observed that an envelope flame could not be supported at velocities above 45 cm/s in their experiments. The experiments were conducted in air at atmospheric pressure and temperature. A drop tower was used to generate microgravity conditions. The conditions in the experiment were simulated by using $T_\infty = 300\,\mathrm{K}$, $p_\infty = 1\,\mathrm{atm}$, and $g = 0$ in the numerical model. Based on these input conditions, the numerical model predicts an extinction velocity of 40 cm/s for $d = 1.3\,\mathrm{mm}$.

Numerical results are presented for a 1.3-mm-diameter *n*-heptane droplet burning in air at a pressure of 1 atm and under zero-gravity ($g = 0$) conditions. The effect of the diffusion velocity formulation on the numerical results for envelope flames is examined by considering three methods for evaluating the diffusion velocity. The three methods are: (a) Fick's law with all binary diffusion coefficients being equal and no thermal diffusion ($\vec{\mathbf{W}}_i = 0$), (b) multicomponent ordinary diffusion with no thermal diffusion ($\vec{V}_i = \vec{\mathbf{V}}_i$), and (c) the full multicomponent formulation with thermal diffusion. In method (a), the binary diffusion coefficient for the fuel–oxygen species pair is used for the single diffusion coefficient ($\mathrm{D}_{ij} = \mathrm{D}_{fo}$). Results for the extinction velocity ($U_{\infty,e}$) and results at a fixed Reynolds number ($\mathrm{Re}_\infty = dU_\infty/\nu_\infty = 10$) are presented below for two different ambient temperatures, $T_\infty = 300$ and $T_\infty = 1,200\,\mathrm{K}$.

Table 1 gives the numerical results for the extinction velocity, Reynolds number at extinction, maximum temperature along the upstream axis of symmetry [$T_{max}(\theta = 0)$], and the stagnation-point flame distance from the droplet surface at extinction [$y_e(0)$] for the two ambient temperatures considered. For $T_\infty = 300\,\mathrm{K}$, our numerical model predicts an extinction velocity of 17 cm/s using method (a) and an extinction velocity of 40 cm/s using methods (b) and (c). The inclusion of multicomponent ordinary diffusion in methods (b) and (c) results in a large increase in $U_{\infty,e}$, and therefore a large decrease in $y_e(0)$, for the $T_\infty = 300\,\mathrm{K}$ case. At this low ambient temperature, the results in Table 1 indicate that thermal diffusion, which is included in method (c), has no effect on the predicted extinction velocity and only a minor effect on $T_{\max}(\theta = 0)$ and $y_e(0)$.

Extinction of an envelope flame occurs somewhere near the forward stagnation point. Figures 3*a* and 3*b* show the species mass fractions and temperature distribution along the upstream axis of symmetry for the $T_\infty = 300\,\mathrm{K}$ case at extinction.

Table 1. Extinction results for $d = 1.3$-mm droplet; $T_\infty = 300$ and $1,200\,\mathrm{K}$

Method	$U_{\infty,e}\,(\mathrm{m/s})$	$\mathrm{Re}_{\infty,e}$	$T_{\max}(\theta = 0)(\mathrm{K})$	$y_e(0)(\mathrm{mm})$
$T_\infty = 300\,\mathrm{K}$				
(a)	0.17	14.1	1,458	0.913
(b)	0.40	33.2	1,744	0.637
(c)	0.40	33.2	1,733	0.632
$T_\infty = 1{,}200\,\mathrm{K}$				
(a)	3.21	25.6	1,793	0.274
(b)	3.76	30.0	1,948	0.261
(c)	3.70	29.5	1,968	0.266

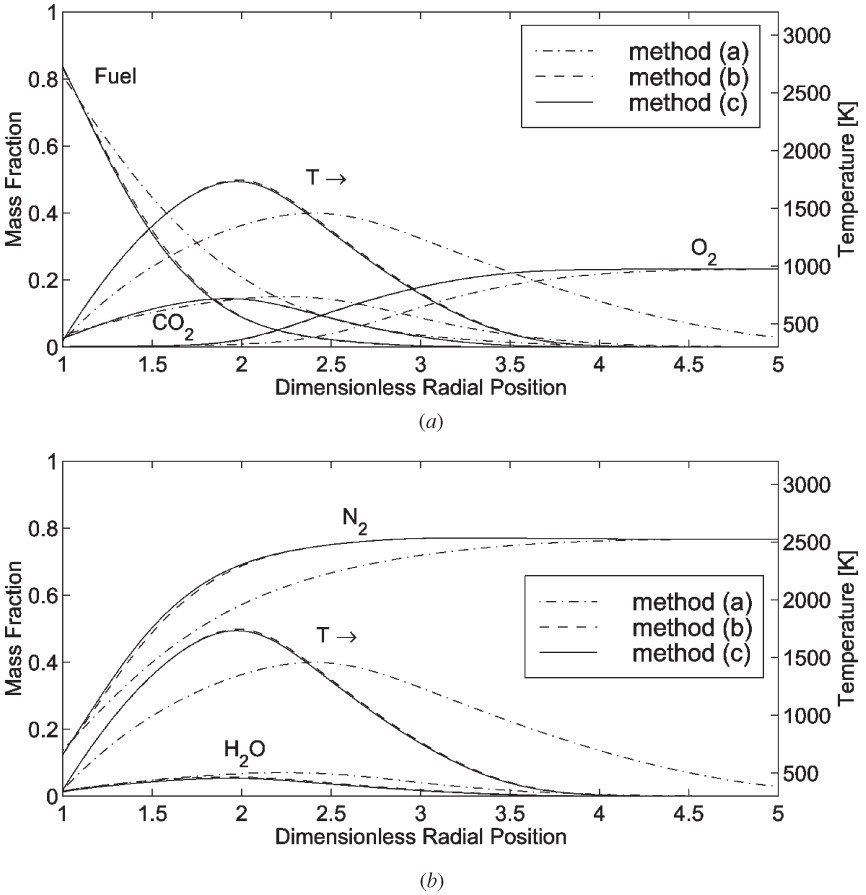

Figure 3. Species mass fractions and temperature distribution along the upstream axis of symmetry for a $d = 1.3$-mm droplet at extinction; $T_\infty = 300\,\mathrm{K}$: (*a*) T and Y_i for fuel, O_2 and CO_2; (b) T and Y_i for H_2O and N_2.

The profiles shown in the figure are similar to extinction results for higher ambient temperatures. The results for methods (b) (dashed line) and (c) (solid line) are almost identical, since extinction occurs at the same velocity and thermal diffusion has only a minor effect. Thermal diffusion causes a slight difference in the predicted fuel mass fractions for methods (b) and (c) as shown in Figure 3*a*. The highest fuel concentrations exist in the region between the droplet surface and the location of the maximum temperature (flame front). In this region, the temperature gradient is positive. The thermal diffusion coefficient for the fuel ($D_{T,f}$) is also positive, resulting in a thermal diffusion velocity for the fuel ($\vec{\mathbf{W}}_f$) that is directed toward the droplet. Thus, the fuel mass fraction from method (c) is shifted toward the droplet when compared to the method (b) results. Figure 3*a* also shows a significant leakage of oxygen and fuel through the flame front at extinction, regardless of the method used to evaluate the diffusion velocity.

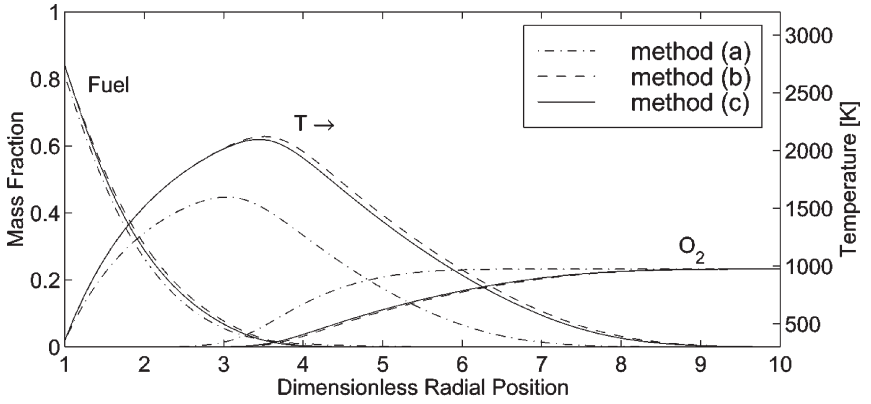

(*a*)

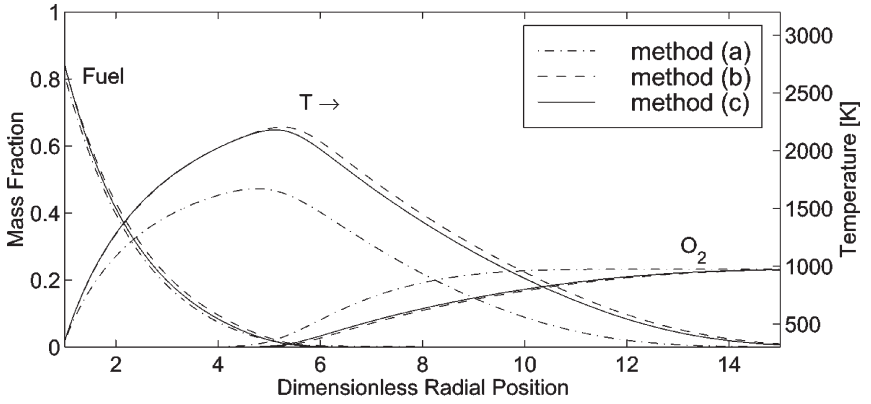

(*b*)

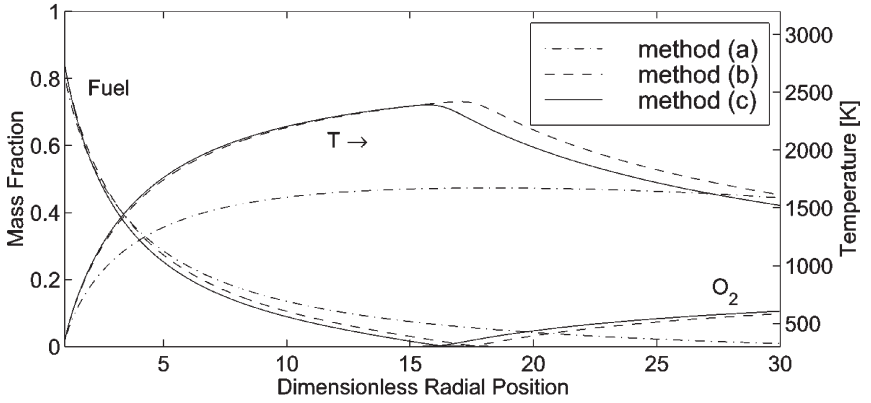

(*c*)

Figure 4. Fuel and O_2 mass fractions and temperature distribution surrounding a $d = 1.3$-mm droplet at $\mathrm{Re}_\infty = 10$; $T_\infty = 300\,\mathrm{K}$: (*a*) $\theta = 0°$; (*b*) $\theta = 90°$; and (*c*) $\theta = 180°$.

Table 1 also gives extinction conditions for the $T_\infty = 1{,}200\,\mathrm{K}$ case. At this higher ambient temperature, method (a) again predicts a lower extinction velocity than methods (b) and (c). Thermal diffusion causes a slight decrease in the extinction velocity between methods (b) and (c). The effect of thermal diffusion becomes noticeable at this higher temperature because of the increase in $T_{\max}(\theta = 0)$ and the decrease in $y_e(0)$ for this case when compared to the $T_\infty = 300\,\mathrm{K}$ case (see Table 1). These changes result in a much higher temperature gradient and therefore higher thermal diffusion velocities for the $T_\infty = 1{,}200\,\mathrm{K}$ case. For both ambient temperatures, method (a) predicts a significantly lower $T_{\max}(\theta = 0)$ (approximately 150 K) than methods (b) and (c).

Figures 4*a*–4*c* show the radial distribution of the temperature and fuel and oxygen mass fractions at three different angular locations for the $T_\infty = 300\,\mathrm{K}$ case with $\mathrm{Re}_\infty = 10$. The figures show that method (a) predicts much lower temperatures than methods (b) and (c). The points of maximum temperature predicted by method (a) deviate substantially from those predicted by methods (b) and (c). In the upstream region (Figure 4*a*), method (a) underpredicts the location of the maximum temperature ($r_f^* = 3.04$) when compared to methods (b) ($r_f^* = 3.51$) and (c) ($r_f^* = 3.44$). In the downstream region (Figure 4*c*), method (a) predicts a more gradual temperature change and a longer ($r_f^* = 18.2$) flame than methods (b) ($r_f^* = 17.0$) and (c) ($r_f^* = 15.7$). Method (a) results in a slightly lower value for the fuel mass fraction at the droplet surface and a much lower temperature gradient at the droplet surface than the other two methods. The inclusion of thermal diffusion in method (c) causes the temperature profile to shift toward the droplet. The temperature and species mass fraction profiles shown in Figures 4*a*–4*c* are typical of results obtained for a fixed Reynolds number.

Table 2 shows the predicted evaporation constant (K), the maximum temperature ($T_{\max}$), and the pressure (C_P), friction (C_F), thrust (C_T), and total (C_D) drag coefficients for the $T_\infty = 300\,\mathrm{K}$ case and the $T_\infty = 1{,}200\,\mathrm{K}$ case with $\mathrm{Re}_\infty = 10$. The higher temperature gradient at the droplet surface for methods (b) and (c) causes an increase in K when compared to method (a). For the $T_\infty = 300\,\mathrm{K}$ case, methods (b) and (c) predict much higher values for K (approximately 20%), C_P (approximately 22%), and C_D (approximately 17%) than method (a). The increase in K, C_P, and C_D is less pronounced (less than 8%) for the $T_\infty = 1{,}200\,\mathrm{K}$ case. At both ambient temperatures, methods (b) and (c) give a maximum temperature ($T_{\max}$) that is approximately 700 K higher than method (a).

Table 2. Results for $d = 1.3$-mm droplet at $\mathrm{Re}_\infty = 10$; $T_\infty = 300$ and 1,200 K

Method	$K(\mathrm{mm}^2/\mathrm{s})$	C_P	C_F	C_T	C_D	$T_{\max}(\mathrm{k})$
$T_\infty = 300\,\mathrm{K}$						
(a)	0.857	3.733	1.121	0.166	5.020	1,704
(b)	1.023	4.546	1.096	0.208	5.849	2,420
(c)	1.036	4.595	1.090	0.207	5.892	2,392
$T_\infty = 1{,}200\,\mathrm{K}$						
(a)	1.621	1.640	0.349	0.029	2.018	2,409
(b)	1.726	1.727	0.328	0.033	2.089	3,114
(c)	1.746	1.753	0.328	0.034	2.114	3,087

6. CONCLUSIONS

A new multicomponent formulation has been presented. The new formulation is appropriate for use with the finite-volume method and includes both multicomponent ordinary diffusion and thermal diffusion (Soret effect). The combustion of a 1.3-mm-diameter *n*-heptane droplet in air at a pressure of 1 atm and under zero gravity was studied using a quasi-steady numerical model. Results obtained using the complete multicomponent formulation were compared to the results obtained while assuming (1) thermal diffusion is negligible and (2) thermal diffusion is negligible and all binary diffusion coefficients are the same. The effect these assumptions had on the extinction velocity and on the results at a fixed Reynolds number ($\mathrm{Re}_\infty = 10$) was investigated for a low (300 K) and a high (1,200 K) ambient temperature.

The use of Fick's law with a single binary diffusion coefficient produced results that were significantly different from the results obtained using the complete formulation. At extinction, the single diffusion coefficient assumption gave a much lower extinction velocity and maximum flame temperature. The results for $\mathrm{Re}_\infty = 10$ showed a reduction in the evaporation constant and drag coefficient of approximately 20% and 17%, respectively, for the low ambient temperature (300 K) case and 8% and 5%, respectively, for the high ambient temperature (1,200 K) case. Maximum temperatures were about 700 K lower at both ambient temperatures when a single binary diffusion coefficient was employed.

Thermal diffusion caused only minor changes in the numerical predictions. The presence of thermal diffusion caused a small (less than 2%) reduction in the extinction velocity for the high ambient temperature case but had no effect on extinction velocity for the low ambient temperature case. At a fixed Reynolds number, thermal diffusion caused; a minor shift of the temperature distribution toward the droplet, a small reduction in the maximum temperature ($\sim$30 K) and an increase in the evaporation constant and drag coefficient of approximately 1%.

The numerical model employed in this study utilizes a one-step overall reaction to model combustion. A more detailed chemical kinetics mechanism can be used to more precisely determine the effects of each of the assumptions discussed above. However, the results of the current study clearly show that multicomponent ordinary diffusion must be included to model droplet combustion adequately.

REFERENCES

1. F. A. Williams, *Combustion Theory*, 2d ed., chap. 1, Benjamin/Cummings, Menlo Park, CA, 1985.
2. S. V. Patankar, *Numerical Heat Transfer and Fluid Flow*, chaps. 2–7, Hemisphere, Washington, DC, 1980.
3. L. W. Huang and C. H. Chen, Flame Stabilization and Blowoff over a Single Droplet, *Numer. Heat Transfer A*, vol. 27, pp. 53–71, 1995.
4. T. Takeda and M. Hishida, Studies on Molecular Diffusion and Natural Convection in a Multicomponent Gas System, *Int. J. Heat Mass Transfer*, vol. 39, pp. 527–536, 1996.
5. R. B. Bird, W. E. Stewart, and E. N. Lightfoot, *Transport Phenomena*, pp. 567–572, Wiley, New York, 1960.

6. S. R. Turns, *An Introduction to Combustion: Concepts and Applications*, 2d ed., pp. 221–223, McGraw-Hill, New York, 2000.
7. E. S. Oran and J. P. Boris, Detailed Modelling of Combustion Systems, *Prog. Energy Combustion Sci.*, vol. 7, pp. 1–72, 1981.
8. E. S. Oran and J. P. Boris, *Numerical Simulation of Reactive Flow*, pp. 253–255, Elsevier Science, San Diego, CA, 1987.
9. T. P. Coffee and J. M. Heimerl, Transport Algorithms for Premixed, Laminar Steady-State Flames, *Combustion and Flame*, vol. 43, pp. 273–289, 1981.
10. D. N. Pope, Numerical Simulation of Convective Fuel Droplet Vaporization and Combustion in a Low Pressure Zero-Gravity Environment, Ph.D. thesis, University of Nebraska—Lincoln, Lincoln, NE, 2001.
11. C. K. Law, Recent Advances in Droplet Vaporization and Combustion, *Prog. Energy Combustion Sci.*, vol. 8, pp. 171–201, 1982.
12. R. Seiser, L. Truett, D. Trees, and K. Seshadri, Structure and Extinction of Nonpremixed *n*-Heptane Flames, *Proc. Combustion Inst.*, vol. 27, pp. 649–657, 1998.
13. R. C. Reid, J. M. Prausnitz, and B. E. Poling, *The Properties of Gases and Liquids*, chaps. 7–11, McGraw-Hill, New York, 1987.
14. T. H. Chung, M. Ajlan, L. L. Lee, and K. E. Starling, Generalized Multiparameter Correlation for Nonpolar and Polar Fluid Transport Properties, *Ind. Eng. Chem. Res.*, vol. 27, pp. 671–679, 1988.
15. C. R. Wilke, A Viscosity Equation for Gas Mixtures, *J. Chem. Phys.*, vol. 18, pp. 517–519, 1950.
16. B. J. McBride, G. Sanford, and M. A. Reno, Coefficients for Calculating Thermodynamic and Transport Properties of Individual Species, NASA Tech. Memo. 4513, October, 1993.
17. J. O. Hirschfelder, C. F. Curtiss, and R. B. Bird, *Molecular Theory of Gases and Liquids*, chap. 8, Wiley, New York, 1954.
18. G. Dixon-Lewis, Flame Structure and Flame Reaction Kinetics, II. Transport Phenomena in Multicomponent Systems, *Proc. Roy. Soc. Lond., Ser. A*, vol. 307, pp. 111–135, 1968.
19. J. D. Ramshaw, Hydrodynamic Theory of Multicomponent Diffusion and Thermal Diffusion in Multitemperature Gas Mixtures, *J. Non-Equilib. Thermodyn.*, vol. 18, pp. 121–134, 1993.
20. P. D. Neufeld, A. R. Janzen, and R. A. Aziz, Empirical Equations to Calculate 16 of the Transport Collision Integrals $\Omega^{(l,s)^*}$ for the Lennard-Jones (12–6) Potential, *J. Chem. Phys.*, vol. 57, pp. 1100–1102, 1972.
21. R. J. Haywood, Variable–Property, Blowing and Transient Effects in Convective Droplet Evaporation with Internal Circulation, M.A.Sc. thesis, University of Waterloo, Waterloo, Ont., 1986.
22. J. P. VanDoormaal and G. D. Raithby, Enhancements of the SIMPLE Method for Predicting Incompressible Fluid Flows, *Numer. Heat Transfer*, vol. 7, pp. 147–163, 1984.
23. M. Vinokur, On One-Dimensional Stretching Functions for Finite-Difference Calculations, *J. Comput. Phys.*, vol. 50, pp. 215–234, 1983.
24. G. A. Agoston, H. Wise, and W. A. Rosser, Dynamic Factors Affecting the Combustion of Liquid Spheres, *Proc. Combustion Inst.*, vol. 6, pp. 708–717, 1957.
25. S. R. Gollahalli and T. A. Brzustowski, Experimental Studies on the Flame Structure in the Wake of a Burning Droplet, *Proc. Combustion. Inst.*, vol. 14, pp. 1333–1344, 1973.
26. K. A. Cliffe and D. A. Lever, A Finite-Element Study of Isothermal, Laminar Flow past a Sphere at Low and Intermediate Reynolds Numbers, Tech. Rep. AERE-R10868, Theoretical Physics Division, AERE, Harwell, Oxfordshire, August 1983.
27. B. Fornberg, Steady Viscous Flow Past a Sphere at High Reynolds Numbers, *J. Fluid Mech.*, vol. 190, pp. 471–489, 1988.

28. A. E. Hamielec, T. W. Hoffman, and L. L. Ross, Numerical Solution of the Navier-Stokes Equation for Flow past Spheres: Part 1. Viscous Flow around Spheres with and without Radial Mass Efflux, *AIChE J.*, vol. 13, pp. 212–219, 1967.
29. N. N. Sayegh and W. H. Gauvin, Numerical Analysis of Variable Property Heat Transfer to a Single Sphere in High Temperature Surroundings, *AIChE J.*, vol. 25, pp. 522–534, 1979.
30. S. R. R. Dennis and J. D. A. Walker, Calculation of the Steady Flow past a Sphere at Low and Moderate Reynolds Numbers, *J. Fluid Mech.*, vol. 48, pp. 771–789, 1971.
31. R. Clift, J. R. Grace and M. E. Weber, *Bubbles, Drops, and Particles*, chap. 5, Academic Press, New York, 1978.
32. S. Taneda, *J. Phys. Soc. Japan*, vol. 11, pp. 1104–1108, 1956.
33. K. A. Cliffe and D. A. Lever, Isothermal Flow past a Blowing Sphere, Tech. Rep. TP.1042, Theoretical Physics Division, AERE, Harwell, Oxfordshire, May 1984.
34. B. P. LeClair, A. E. Hamielec, H. R. Pruppacher, and W. D. Hall, A Theoretical and Experimental Study of the Internal Circulation in Water Drops Falling at Terminal Velocity in Air, *J. Atmos. Sci.*, vol. 29, pp. 728–740, 1972.
35. C. H. Chiang, M. S. Raju, and W. A. Sirignano, Numerical Analysis of Convecting, Vaporizing Fuel Droplet with Variable Properties, *Int. J. Heat Mass Transfer*, vol. 35, pp. 1307–1324, 1992.
36. M. Renksizbulut and M. C. Yuen, Numerical Study of Droplet Evaporation in a High-Temperature Stream, *J. Heat Transfer*, vol. 105, pp. 389–397, 1983.
37. M. Renksizbulut and M. C. Yuen, Experimental Study of Droplet Evaporation in a High-Temperature Air Stream, *J. Heat Transfer*, vol. 105, pp. 384–388, 1983.
38. D. N. Pope and G. Gogos, Numerical Simulation of Fuel Droplet Extinction due to Forced Convection, *Combustion and Flame*, vol. 142, pp. 89–206, 2005.
39. D. N. Pope, D. Howard, K. Lu, and G. Gogos, Combustion of Moving Droplets and Suspended Droplets: Transient Numerical Results, *J. Thermophys. Heat Transfer*, in press, 2005.
40. S. R. Gollahalli and T. A. Brzustowski, The Effect of Pressure on the Flame Structure in the Wake of a Burning Hydrocarbon Droplet, *Proc. Combustion Inst.*, vol. 15, pp. 409–417, 1975.
41. M. Goldsmith, Experiments on the Burning of Single Drops of Fuel, *Jet Propulsion*, vol. 26, pp. 172–178, 1956.
42. S. Okajima and S. Kumagai, Experimental Studies on Combustion of Fuel Droplets in Flowing Air under Zero- and High-Gravity Conditions, *Proc. Combustion Inst.*, vol. 19, pp. 1021–1027, 1982.